Desalination and Water Treatment
www.deswater.com

doi: 10.5004/dwt.2019.23868

155 (2019) 1–14
July

Enhanced performance of forward osmosis membranes by incorporating PVDF substrates with hydrophilic nanofillers

Hui-Min Cui, Xi Yan, Yan Chen*, Wen-Yan Xu, Wan-Zhong Lang*

The Education Ministry Key Laboratory of Resource Chemistry and Shanghai Key Laboratory of Rare Earth Functional Materials, College of Chemistry and Materials Science, Shanghai Normal University, 100 Guilin Road, Shanghai 200234, China, Tel. +8613570253780; email: ychen@shnu.edu.cn (Y. Chen), Tel. +8613917278949; email: wzlang@shnu.edu.cn (W.-Z. Lang), Tel. +8613636523463; email: 15312323920@163.com (H.-Min Cui), Tel. +8618602185275; email: yanxi@shnu.edu.cn (X. Yan), Tel. +8618930289346; email: xwy@shnu.edu.cn (W.-Y. Xu)

Received 9 July 2018; Accepted 26 January 2019

ABSTRACT

Hydrophilic attapulgite (AT) and functional oxidized multi-walled carbon nanotubes (O-MWCNTs) are introduced to the polyvinylidene fluoride (PVDF) substrates to prepare improved performance of thin-film composite (TFC) membranes for forward osmosis (FO) process. The improved hydrophilicity of substrates can make for forming free-defect polyamide (PA) layer and enhance the permeability performance of the as-prepared TFC membranes. The effects of the single or composite addition of two nanofillers on the hydrophilicity, membrane morphology, porosity and mechanical strength of as-prepared substrates are investigated in detail. The results show that hydrophilic, porous and high-flux substrates are prepared and the corresponding TFC membranes own improved water flux and better selectivity. In a word, the PVDF/AT/O-MWCNTs TFC membrane receives a better water flux (J_v) of 28.23 and 20.37 L.m^{-2}.h^{-1} and a lower reverse salt flux (J_s) of 9.5 and 6.5 g.m^{-2}.h^{-1} in pressure-retarded osmosis (PRO) mode (active layer facing draw solution, AL-DS) and FO mode (active layer facing feed solution, AL-FS). The draw solution and feed solution are 2M NaCl aqueous solution and deionized (DI) water, respectively. This study develops a brand-new way for preparing substrate for FO process.

Keywords: Polyvinylidenefluoride (PVDF); Forward osmosis membrane; Attapulgite; Oxidized multi-walled carbon nanotubes (O-MWCNTs)

1. Introduction

Nowadays, the water shortage seriously threatens the survival of human beings' living and development of economy [1–3]. Lately, forward osmosis (FO) process works with lower external pressure while the reverse osmosis (RO) process is widely used to produce pure water as an advanced and energy-saving technology [4–7]. FO process shows excellent superiority of high water recovery being possible, lower fouling tendency and with lower energy consumption while other osmosis-driven separation processes are opposite to FO process, for instance, nanofiltration (NF) and reverse osmosis (RO) [8,9].

The thin-film composite (TFC) membrane generally has a thin skin layer and a porous and hydrophilic substrate and this structure endows them with higher water flux, better mechanical strength, preferable salt rejection, secular stability and good adjustability in FO process[10,11]. The highly porous and hydrophilic substrates with appropriate mechanical strength can receive relatively improved water flux and standing stability, and this structure is of help to form free-defect active layer formed by click reaction of interfacial polymerization (IP) reaction. The two reactive monomers are trimesoyl chloride organic solution and p-phenylenediamine hydrochloride aqueous solution.

* Corresponding authors.

Large amounts of studies have been investigated thoroughly to polish up the polyamide (PA) layer with a well-distributed and denser surface by altering reactive monomers or adding different hydrophilic nanofillers into amine solution or into organic solution[10,12–14]. The substrates also play important roles in the property of the as-prepared TFC membrane and some research findings were obtained in the previous works [15–19].

The polymer materials used as FO substrates are in a wide range of cellulose acetate [20,21], polysulfone (PSF) [19,22–24], polyether sulfone (PES) [13,16,25,26], and polyacrylonitrile (PAN) [27] to obtain highly porous support. Among polymer materials for fabrication of membranes, polyvinylidene fluoride (PVDF) owns excellent thermal and chemical stability, better mechanical performance and so on. Through the PVDF has so many advantages, the pure PVDF membrane with intrinsic hydrophobicity hinders its further application in the water treatment process. In FO process, in order to receive higher water flux, it's essential to prepare a hydrophilic substrate with a great deal of large pores, lower structure parameter and better hydrophilicity, which can promote the IP reaction and decrease the inter concentration polarization (ICP) effects on the membrane performance [11,28]. From previous work, we can see some study has been contributed to improve the substrate performance via incorporating hydrophilic organics [29,30], inorganic nanoparticles [15,17,23], pore forming agents [22,23], or different organic solvent [14,19] and so on. Moreover, there are works turning to the hydrophilic modification based on the commercial membrane as substrate, for example, surface grafting [31], blending modification [32,33], and surface modification [15], layer-by-layer assembly [34,35] and so on. The as-prepared TFC membranes in previous work all showed improved water flux, outstanding solute rejection and excellent anti-fouling property.

In this work, we research the effects of blending addition of two hydrophilic nano-materials into the dope solution on preparing porous and hydrophilic substrates. The multi-walled carbon nanotubes (MWCNTs) have entered the researchers' vision due to their unique properties, such as its improved physical properties including mechanical strength and tensile moduli, and it has been used as additives in the forming of the substrates in previous work [36–38]. Attapulgite (AT) is made of hydrated magnesium aluminum silicate which has a chain-like structure by layer. As we all know, AT is one of plentiful and ten-cent clay minerals and it owns ample hydroxyl groups including Mg–OH, Al–OH and Si–OH, and it can seldom be seen in the TFC membrane process from the previous work [39]. The hydrophilic groups are gathered on the top surface of substrates under strong hydrogen bond among carboxyl groups, hydroxyl groups and water molecules during phase separation to obtain hydrophilic substrates. In our study, we use functional oxidized multi-walled carbon nanotubes (O-MWCNTs) with large amounts of carboxyl groups and AT to modify the PVDF substrates by single modification and blending modification of both to prepare substrates and then to form free-defect selective layer. And this work may offer a method to design brand-new TFC membranes on the support membranes prepared by blending modification of hydrophilic nanofillers.

2. Experimental

2.1. Materials

Polyvinylidene fluoride (PVDF, Solef 1015) was bought from Solvay Advanced Polymers. N-hexane and sodium chloride (NaCl), N-methyl pyrrolidone (NMP) worked as solvent, and other chemicals were bought from Shanghai Chemical Agent Company (China). Polyvinylpyrrolidone (PVP Mw = 58000 Da) worked as pore-forming agent was bought from Shanghai Aladdin Chemical Agent Co. Ltd (China). 1,3,5-benzenetricarbonyl trichloride (TMC, 98%) and p-phenylenediamine (PPD) hydrochloride by IP reaction used as selective layer were bought from Shanghai Aladdin Chemical Agent Co. Ltd (China). Pristine MWCNTs with a diameter of 20–40 nm and average length of 5–15 μm were bought from Shenzhen Nanotech Port Co. Ltd (China). Attapulgite (AT) nanoclay (99.8% purity, ρ = 2.05 g·cm^{-3}) was purchased from Jiangsu Jiuchuan Nano-Material Technology Co., China. Deionized (DI) water was prepared by laboratory-made.

2.2. Modification of MWCNTs

Before modification, 1.0 g of pristine MWCNTs was purified by 0.5 mol·L^{-1} of HCl. And then, dry MWCNTs was dispersed in a vessel which was added into mixed acid (the volume ratio of sulfuric to nitric acid is 3:1) [20]. The suspension obtained kept stirring at 70°C for about 6 h. After that the mixture was cooled using ice bath. Functional oxidized MWCNTs (O-MWCNTs) were obtained by centrifugal separation, and then washed with DI water. Then, the O-MWCNTs were dispersed in DI water to make the solution of a pH of 7 and then obtained by vacuum filtration further. Finally, the resulting O-MWCNTs was vacuum dried in an oven for 12 h at 70°C before used.

2.3. Preparation of PVDF/AT/O-MWCNTs substrates

The PVDF/AT/O-MWCNTs casting solutions were prepared from pre-weighted PVDF, PVP, O-MWCNTs/AT and balanced NMP solvent, and kept stirring at 70°C for 12 h, and degassed for 24 h. The detailed composition of casting solutions for the substrates is shown in Table 1. The uniform dope solution was cast on a clean glass plate. The casting knife with 100 μm height was used to roll out the dope solution. The substrates were then got by Non-solvent Induce Phase Separation (NIPS) method. The fabricated substrates were stored in DI water, and the DI water was replaced every 12 h. The substrates containing

Table 1
Dope compositions for PVDF substrates

Substrate no.	PVDF (wt.%)	PVP (wt.%)	NMP (wt.%)	O-MWCNTs (wt.%)	AT (wt.%)
M0	16.0	2.0	82.0	/	/
MA	16.0	2.0	81.5	/	0.5
MC	16.0	2.0	81.0	1.0	/
MAC	16.0	2.0	80.5	1.0	0.5

different additives were denoted as M0 (control membrane), MA (0.50 wt.% of AT), MC (1.0 wt.% of O-MWCNTs) and MAC (0.5 wt.% of AT and 1.0 wt.% of O-MWCNTs), respectively. And their corresponding TFC membranes are FO-M0, FO-MA, FO-MC and FO-MAC, respectively.

2.4. Preparation of TFC membrane

The PA selective layer of TFC membrane was fabricated by IP reaction between PPD molecules and TMC molecules on the top surface of the substrate fixed in a clean frame. The concentration of PPD aqueous solution was immobilized at 3.00 wt.% and was tiled onto the top surface of earlier-mentioned support and kept for 2 min. Then, the superfluous PPD aqueous solution was wiped off the substrate using tissue paper. Then, humid membranes with amine solution fixed in frame was dropped into a 0.15 wt.% of TMC in n-hexane solution for 1 min to fabricate the PA selective layer. Finally, the fabricated TFC membranes were dried at room temperature for several minutes. After that, the TFC membrane were washed by water to remove some unreactive groups and stored in DI water for further tests.

2.5. Characterizations of additives and membranes

The chemical composition of O-MWCNTs powder was detected using Fourier transform infrared spectra (FTIR, Lambda Scientific Pty Ltd) made in Australia to detect the functional groups of MWCNTs at 800–4,000 cm^{-1}. The element compositions of top surfaces of TFC membranes were analyzed by an X-ray photoelectron spectroscopy (XPS, PHI 5000C ESCA) made in USA.

The surface and cross-sectional morphology photos of all substrates and TFC membranes were taken by a field emission scanning electron microscopy (FESEM, Hitachi S-4800) made in Japan. The clear cross-sections of all membranes were fractured in liquid nitrogen.

Furthermore, surface roughness of prepared membranes including substrates and TFC membranes were detected by atomic-force microscopy (AFM, Technologies-5500) made in USA. Surface roughness of all membranes was investigated by average surface roughness (R_a) and root mean square roughness (R_q). All membrane samples were studied at 25°C with scanning size of 3 × 3 μm at a speed of 2 Hz.

The wettability of PVDF hybrid substrates were investigated by sessile drop method with a contact angle instrument (DSA30, German) loaded with camera video at 25°C. Dry PVDF substrate was attached onto slide glasses. A drop of 3.0 μL of water was dropped at room temperature and the results during the test time were recorded by a camera, and the images could reveal the real time of the contact angle. The mechanical properties of as-prepared substrates were examined with a stretching rate at the same rate by a test machine (QJ210A, Shanghai Qingji Instrumentation Sci. & Tech. Co., Ltd) made in Shanghai of China.

The membrane porosity (ε) was obtained by the gravimetric method, the equation is:

$$\varepsilon = \frac{\dfrac{(\omega_1 - \omega_2)}{\rho_{water}}}{\dfrac{(\omega_1 - \omega_2)}{\rho_{water}} + \dfrac{\omega_2}{\rho_P}} \times 100\% \quad (1)$$

where ε (%) is used to illustrate the porosity of the membranes, ω_1 (g) represents the wet membrane's weight, ω_2 (g) is the dried membrane's weight, ρ_P (g/cm^3) and ρ_{water} (g/cm^3) are the density of PVDF and water at 25°C, respectively (25°C, ρ_P = 1.780 g/cm^3, ρ_{water} = 0.997 g/cm^3).

The average pore radius (r_m, nm) of the support membrane was got via the Guerout–Elford–Ferry, which had links with water flux, membrane porosity and membrane thickness [40], the equation is:

$$r_m = \sqrt{\frac{(2.9 - 1.75\varepsilon) \times 8\eta l J_w}{\varepsilon \Delta P}} \quad (2)$$

where η is the water viscosity and the specific parameter is 1.002×10^{-3} Pa·s, l is the thickness of substrates (m) and ΔP is the transmembrane pressure (bar).

A dead end filtration device was used to test water fluxes J_w of substrates and the valid separation area was 12.56 cm^2. There was a hose between the vacuum pump and the device to connect them with each other. The pure water flux (J_w) of substrate linked with the volume of water permeability, valid separation area and pressure was calculated by the following equation:

$$J_w = \frac{V}{A_m \cdot t \cdot \Delta P} \quad (3)$$

where V (L) is used to represent the volume of permeate, A_m (m^2) is used to represent valid membrane area, ΔP (bar) is used to represent transmembrane pressure and t (h) is used to represent operation time.

2.6. Evaluation of forward osmosis membrane performance

2.6.1. Intrinsic performances of forward osmosis membranes

The cross-flow lab-scale filtration machine was employed to measure pure water permeability coefficient (A) of TFC membranes. All TFC membrane samples with the selective layer facing water were pressured before tests and the pressure is fixed at 2.0 bar for 1 h at 25°C and then the stable performance was tested at 1.0 bar at the same temperature. The water permeability coefficient (A) of the TFC membrane sample was figured out by:

$$A = \frac{V}{A_m \cdot t \cdot \Delta P} \quad (4)$$

The NaCl rejection R was examined in PRO mode. The concentrations of two kinds of solution including the feed solution and permeate were examined by measuring the electrical conductivity.

$$R = \frac{C_f - C_p}{C_f} \times 100 \tag{5}$$

$$C_p = \frac{C_t \times V_t - C_0 \times V_0}{V_t - V_0} \tag{6}$$

where C_p (mol L^{-1}) and C_f (mol L^{-1}) are corresponding to the salt concentrations of two kinds of salt solution including the permeate and feed, respectively. C_t (mol L^{-1}) and C_0 (mol L^{-1}) are final and initial salt concentration, respectively. V_t (L) and V_0 (L) are the final and initial volume, respectively.

The solute permeability coefficient (B) was examined from the FO setup [16]. DI water and 1M NaCl played a role of the feed solution and draw solution, respectively. The test experiment of TFC membrane was carried on in PRO mode, and the B value was calculated by Eq. (7):

$$B = \frac{1}{A_m t\left(\frac{1}{V_d} + \frac{1}{V_f}\right)} \ln\left(\frac{C_d^0 - C_f^0}{C_d^t - C_f^t}\right) \tag{7}$$

where A_m is the effective separation area, V_f (L) and V_d (L) are on behalf of the volume of the feed and draw solution, respectively. And $C_d^0\left(\text{mol}\cdot\text{L}^{-1}\right)$ and $C_f^0\left(\text{mol}\cdot\text{L}^{-1}\right)$ represents the initial concentration of the feed solution and the draw solution monitored by using a conductivity meter and $C_d^t\left(\text{mol}\cdot\text{L}^{-1}\right)$ and $C_f^t\left(\text{mol}\cdot\text{L}^{-1}\right)$ are on behalf of final concentration of the feed solution and draw solution monitored by using a conductivity meter.

2.6.2. Forward osmosis measurement

The FO experimental system was used to evaluate water flux (J_v, L·m^2·h^{-1}) and reverse solute flux (J_s, g·m^2·h^{-1}) of fabricated TFC membranes. Briefly, the draw solution and feed solution are 2M NaCl solution and DI water, respectively, and they work under settled flow rate of 0.30 L min^{-1} during the FO process. The water permeation flowing from feed solution to draw solution was recorded by a digital weight balance, which conveyed data to the computer. After the experiment, the salt concentration of the feed solution side and draw solution side were tested by the conductivity meter. The FO performance was evaluated under two modes. They are FO mode (active layer facing feed solution, AL-FS) and pressure-retarded osmosis (PRO) mode (active layer facing draw solution, AL-DS). Tests of each membrane sample should be gone on for at least three times and obtain the average results. Tests of all samples were carried out for at least 1 h. The water flux (J_v, L·m^2·h^{-1}) and the reverse solute flux (J_s, g·m^2·h^{-1}) were calculated by Eqs. (8) and (9):

$$J_v = \frac{\Delta V}{A_m t} \tag{8}$$

$$J_s = \frac{\Delta\left(C_t V_t\right)}{A_m t} \tag{9}$$

where ΔV (L) is the water volume from the feed solution to the draw solution because of its own osmotic pressure under test time (t), A_m (cm^2) is the valid separation membrane area of 4.18 cm^2, C_t (mol L^{-1}) and V_t (L) are the final salt concentration and volume of the feed solution after tests, respectively. Moreover, different concentrations of draw solution were also discussed to study their effects on J_v and J_s.

3. Results and discussion

3.1. Influences of addition of different nanofillers on substrates

The FESEM photos containing top surface and cross-section of the fabricated PVDF substrates can be seen from Fig. 1. It can be found that four membranes have clear big pores of the cross sections. Pore size and pore numbers vary with different nanofillers, especially MAC has the largest pores among the four membranes. That's due to hydroxyl (–OH) on the surface of AT and carboxyl groups (–COOH) of O-MWCNTs make the membrane more hydrophilic than the single modification membranes. The nano-pores of the top surface of the substrates are usually considered as defects of an ideal membrane and ascribed to the entrances of the finger-like pores. However, they are useful for the improvement of the pure water permeation contributing largely to improve the porosity of the membranes, which can further reduce the ICP and thus lower the membrane tortuosity. MAC owning large pores on the surface may be the existence of strong bonds between large amounts of carboxyl groups grafted to the O-MWCNTs and hydroxyl groups of AT and water molecules during phase separation.

The cross-section morphologies of the as-prepared membrane are shown in the right of Fig. 1. We can see that all membranes have the typical asymmetrical structure with finger-like macro-pores and a dense layer of the top layer. M0 owns irregular macro-pores of the cross-sectional morphology and a part of small pores and the reason is that higher hydrophobicity of PVDF delays the demixing during phase inversion process. Introduction of hydrophilic O-MWCNTs and AT into PVDF substrate make the pore large, regular and uniform. The membrane tortuosity is lower than the control one. The reason for the varied morphologies of the PVDF substrates could be the fact that the massive –COOH and –OH in the oxidized MWCNTs and AT contribute to the solvent exchange during the phase separation. All in all, the hydrophilic nanofillers in the dope solution make for the momentary phase separation and contribute to the formation of more porous substrates [22].

Correspondingly, surface roughness and roughness parameters of the as-prepared substrates are shown in Fig. 2. Results show that the top surface roughness of the fabricated TFC membranes increases as additions of different nanofillers. The results are consistent with the FESEM images. The values of R_a and R_q increase simultaneously, which could be thanks to the incorporation of O-MWCNTs, AT and their composite accelerating the phase separation during the preparation of the substrates. We can also see from the FESEM images that the accelerated phase separation leading to the decreased number of the pores on surfaces of the substrate and the increased surface roughness ranges from M0 to MAC [16].

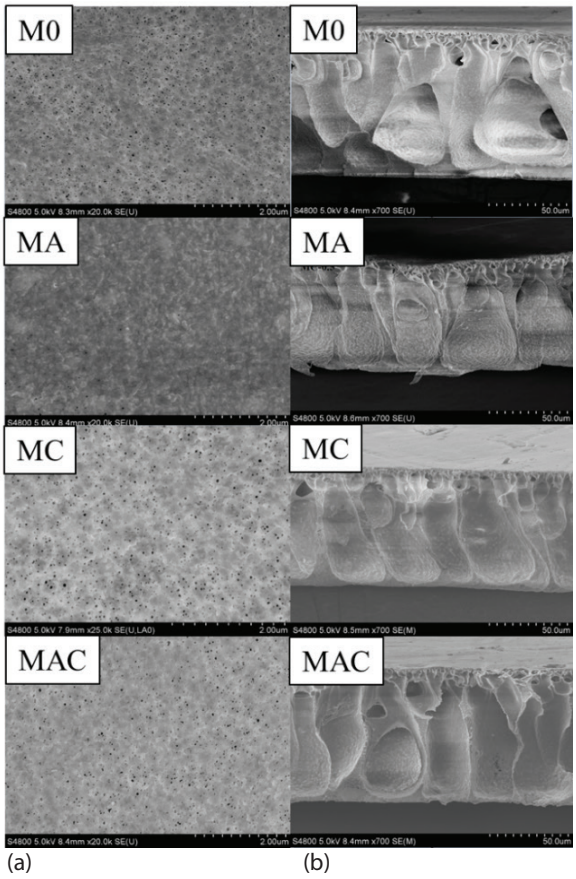

Fig. 1. FESEM images of the top surfaces (a) and cross section (b) of the as-prepared PVDF and PVDF composite substrates.

The surface wettability of the substrates is detected by the dynamic contact angle, and the results are shown in Fig. 3, the contact angle of the substrate decreases from 80.9° of the control membrane M0 to 61.1° of membrane MAC. Normally, the drop of the contact angle states clearly the improvement of the hydrophilicity for the substrates, which conversely leads to higher water permeability [41]. For MA, the abundant hydrophilic groups, for example, water molecules and hydroxyl (–OH) of AT make the membrane more hydrophilic than the control membrane M0. For MC, the addition of O-MWCNTs into the casting membrane solution can remarkably enhance wettability of the PVDF substrate. The reason that the carboxyl groups (–COOH) of the functional MWCNTs can form hydrogen bonds with water molecules. The functional carboxyl groups of O-MWCNTs

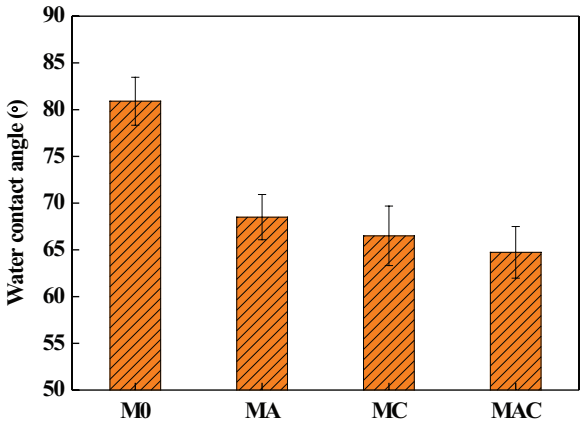

Fig. 3. Water contact angles of PVDF substrates.

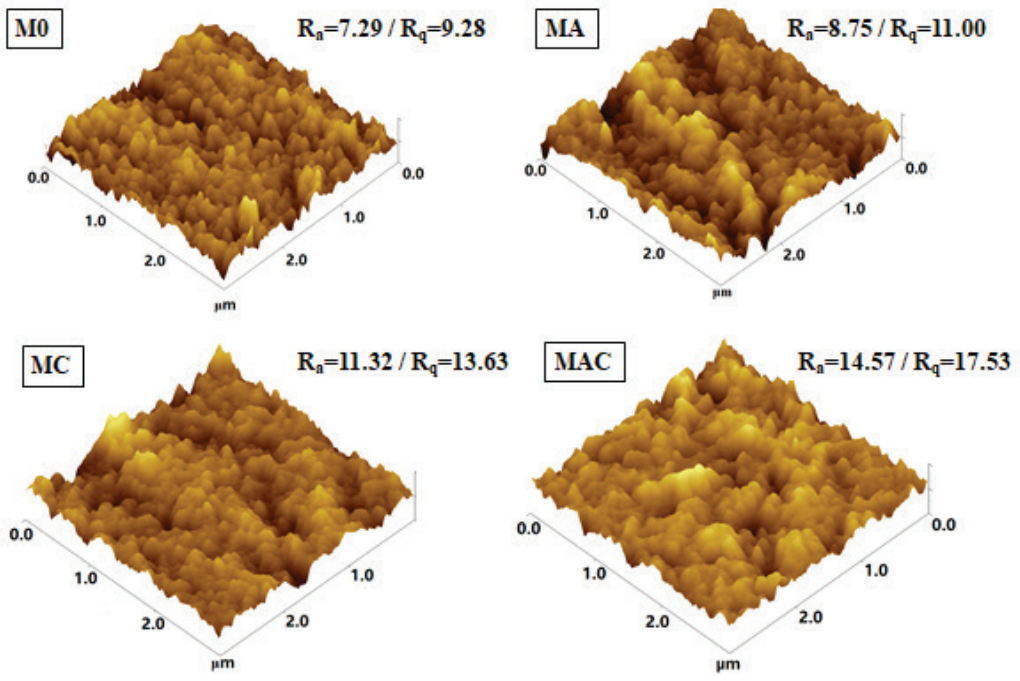

Fig. 2. AFM images of the top surfaces of the substrates.

will be enriched during phase separation process, which makes contact angle be lower. For composite membrane MAC, a great deal of hydrophilic groups (–OH of AT and –COOH of the functional O-MWCNTs) make the membrane be more hydrophilic than the other three membranes. All in all, the blending of AT and O-MWCNTs of MAC works best among them and gains the best hydrophilicity [42,43]. These results indicate the pull-in of functional O-MWCNTs and AT can get overwhelmingly improved hydrophilicity of the substrates.

Fig. 4 shows the porosity ranging from 65.40% of the M0 to 84.20% of the MAC with the different additions into the substrates and the result indicates that the blending of both O-MWCNTs and AT is better for the formation of the large pores than the addition of the single one to improve the membrane performance. The result is consistent with the corresponding morphology variation.

Furthermore, the pore sizes of the PVDF substrates are also illustrated in Fig. 5, which ranges from 34.26 to 38.44 nm. It's clear that pore size of the substrate increases with the rise of the hydrophilicity of the substrates, which is consistent with the membrane morphology and can be attributed to the comprehensive effects of precipitation kinetics and different phase separation processes [1,44]. The smaller pores of the substrates perhaps produce PA layer with smaller water permeability [45], which will be discussed in the following.

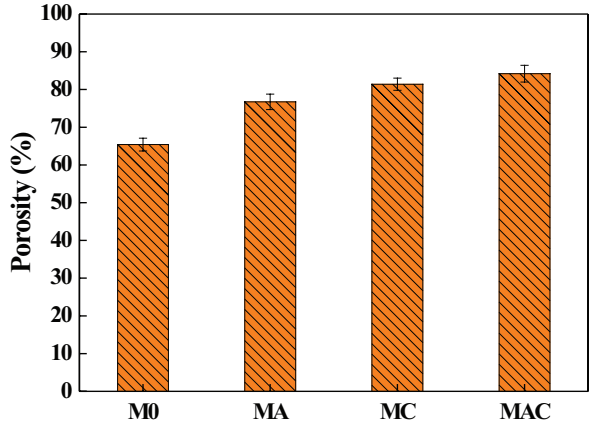

Fig. 4. Porosities of PVDF substrates.

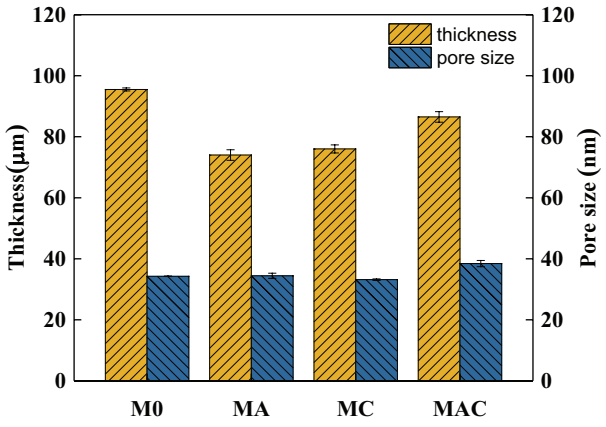

Fig. 5. Thickness and pore size of PVDF substrates.

As shown in Fig. 5, the thickness of the substrates is in a range of 74.00 to 95.50μm, which descends at first and then increases as reported in previous work [46]. The improved contents of hydrophilic groups result in a thinner and more porous membrane since hydrophilic polymers could tolerate the higher water content before the phase separation [1]. However, the enhanced hydrophilicity of the dope solution with the blending of the two additions causes the enhanced phase separation and leads to the larger thickness of the PVDF substrates.

The pure water fluxes (J_w) of the PVDF substrates are shown in Fig. 6. In a word, the porosity and the surface wettability will serious influence water permeability of the substrates. The control PVDF substrate (M0) possesses the lowest permeability of 231.5 $L{\cdot}m^{-2}{\cdot}h^{-1}{\cdot}bar^{-1}$, which is the result of poorer hydrophilicity and its lower porosity. Higher water transport resistance is caused by the irregular macrovoid structure and a part of small pores, which further cuts down the water permeability. The water permeability continuously increases to 509.6 $L{\cdot}m^{-2}{\cdot}h^{-1}{\cdot}bar^{-1}$ of MAC due to the improved hydrophilicity, higher porosity and lower tortuosity of the as-prepared substrates.

The influence of ICP on the FO process can be estimated by the structure parameter S. As shown in Table 2, the improved hydrophilicity, big pore and less tortuosity of the resultant PVDF substrate samples are the result of the *S* values of the as-prepared TFC membranes displaying a decreasing tendency from M0 to MAC. In a word, reduced ICP can be realized by adding hydrophilic nanofillers into the PVDF substrates to improve their hydrophilicity and porosity. The ratio of τ/ε may be a suitable instruction which displays the intrinsic resistance to diffusion supplied by the

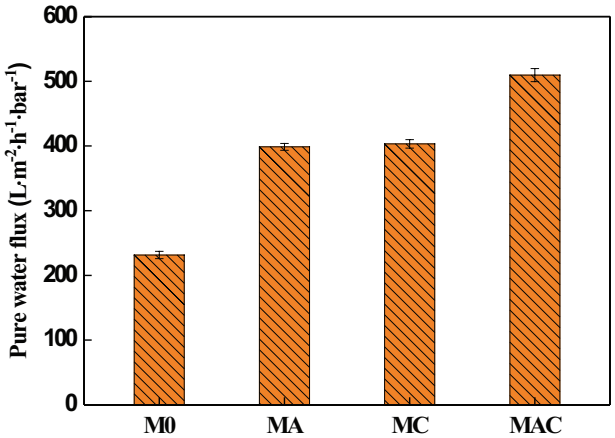

Fig. 6. Pure water flux of PVDF substrates.

Table 2
Intrinsic separation properties of TFC membranes

Membrane no.	S (μm)	τ/ε
FO-M0	1901 ± 31	25.35
FO-MA	1334 ± 14	23.00
FO-MC	913 ± 73	19.85
FO-MAC	621 ± 21	18.81

structure because the result could report how the intrinsic microstructure affects the FO process [47]. As shown in the Table 2, the τ/ε of the TFC membranes decreases from M0 to MAC, which may be due to more open pores formed with the improved surface hydrophilicity of the substrates and much smoother PA layer. In conclusion, higher porosity, improvement of the surface hydrophilicity, and smoother PA selective layer would lead to lowering structure parameter *S* and enhancing water flux.

The introduction of additives to the dope solution has significant effects on the mechanical strength of the as-prepared PVDF substrates. Tensile strength, Young's modulus and elongation at break of the resultant PVDF substrates are exhibited in Table 3. Table 3 demonstrates that three indicators all basically increase from M0 to MAC. AT was successfully dispersed into the polymer matrix, and bonded well with PVDF chain, which provided toughened local regions in the membrane. And this phenomenon stunted the development of cracks and cavities to enhance the mechanic performance of PVDF substrates [42]. The improvement of mechanic performance is the reason for the high strength and interfacial interaction between PVDF polymer matrix and hydrophilic O-MWCNTs. Some reports also verified that the introduction of O-MWCNTs could obviously enhance the mechanical performance of membranes [15,20]. So, the incorporation of hydrophilic additives to the substrates is helpful to raise their mechanical properties. It is likely that the nanofillers could transfer their superior mechanical properties to the polymer matrix. The effectiveness of the functional O-MWCNTs and AT in raising the mechanical properties is successfully testified.

3.2. Influences of modified substrates on PA selective layer

As is shown in Fig 7(a), the new peaks of 1,658 and 1,543 cm^{-1} appeared in TFC membranes are ascribed to the amide functional groups. The peak of 1,658 $cm^{-1}$is ascribed to the C=O stretching vibrations of amide I and the peak of 1,543 cm^{-1} is ascribed to C=O in-plane N–H bending and C–N stretching vibrations of amide II, respectively [3], which proves directly the success of forming PA selective layer on top surface of the substrates. The peaks of 1,402, 1,275, 1,180, 876 and 841 cm^{-1} are ascribed to the characteristic peaks of PVDF. Furthermore, the weak characteristic absorption peaks of PVDF on the PVDF substrates are weakened ranging from the single addition to the composite addition, which shows the improvement of substrate wettability is good for the forming uniform PA selective layer. The elementary compositions of the TFC membrane samples are also identified by the XPS measurement with a wide scan and the results can be seen from Fig 7(b) and Table 4. Fig 7(b) demonstrates that the change of surface chemical composition of the TFC membranes. Three peaks at 531.03, 399.48 and 284.95 eV of the TFC membranes appear which belongs to O, N and C elements, respectively [48]. As is shown in Table 4, the three elements appear and are the same with each other. To sum up, it can be clear got that the PA layer has been immobilized on the four membranes by IP reactions illustrated in Fig. 8.

As shown in Figs. 9 and 10, it's necessary to take surface chemical functional groups of the FO membranes into consideration by the high-resolution narrow-scanned XPS spectra and the results got from the XPS tests are shown in Table 5. Besides, Fig. 9 shows two kinds of peaks, the peak at 531.2 eV is in accordance with O–C=O, N–C=O, and both of two peaks belong to OI. The peak at 532.6 eV is in accord with

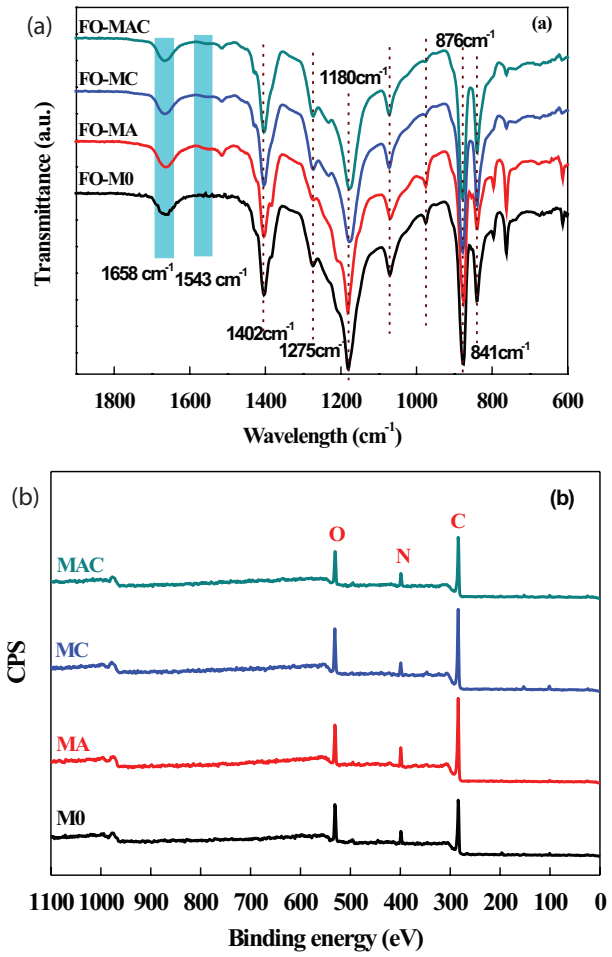

Fig. 7. (a) ATR-FTIR spectra and (b) XPS curves of TFC membranes.

Table 3
Mechanical performance of resultant PVDF substrates

Substrates	Tensile strength (Mpa)	Young's modulus (Mpa)	Breaking elongation (%)
M0	1.71 ± 0.14	28.58 ± 6.64	54.73 ± 1.87
MA	1.81 ± 0.09	33.17 ± 4.11	50.19 ± 9.79
MC	2.23 ± 0.24	43.98 ± 2.25	57.36 ± 5.88
MAC	2.45 ± 0.12	48.26 ± 0.58	65.07 ± 2.65

O–C=O which belongs to OII. Both of OI and OII are involved in the deconvolution of O1s spectra of the FO membranes. For two peaks of O1s, those carboxyl groups transformed from spare acyl chloride groups are the source of the oxygen atoms in O–C=O bond. In a word, as shown in Table 5, the intensity ratio of OI/IOII of resultant TFC membranes decreases from M0 to MAC, which demonstrates that more residual acyl chloride groups of PA selective layer based on the pure substrate have been, hydrolyzes into carboxyl groups. Furthermore, Fig. 10 shows the deconvolution of N1s spectra of TFC membranes. There are two peaks contained in them.

Table 4
Atomic fractions (%) of surface elemental composition of TFC membranes by XPS analysis

Code	M0	MA	MC	MAC
C	73.04	75.18	76.22	73.59
F	0.33	0.51	0.54	0.01
N	7.84	8.38	5.92	7.63
O	18.79	15.93	17.31	18.77

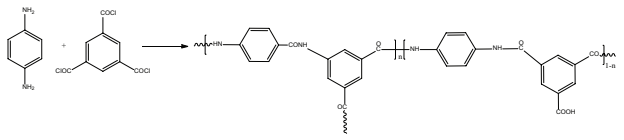

Fig. 8. IP reaction to form thin-film-composite PA membrane.

The binding energy of 400.4 eV is in keeping with O=C–N which belongs to NII and the binding energy of 399.2 eV is in line with C–NH which belongs to NI. The XPS results are perfectly consistent with ATR-FTIR [49].

In Fig. 11, we can see that the top surface on the left and cross sectional on the right of the as-prepared TFC membrane samples based on varied additions of PVDF substrates. The top surface is smooth and dense without obvious pores compared with the substrates, indicating the successful formation of the PA layers. As we all know, the PA layer experiences two stages in the formation process [50]. In the first step, the amino of PPD molecules reacts with the acyl chloride of TMC molecules. This reaction happens at the interface of the aqueous solution and the organic solution. The PA selective layer with smooth structure will be formed during reactive process. In the second step, the migration of PPD molecules toward TMC phase is enhanced, which optimizes the pristine thin selective layer and contributes to form more smooth structure of PA layer under the so-called Marangoni effect. As is shown in right of Fig. 11, the thickness of active layers of resultant TFC membranes were earlier decreases and later increases from M0 to MAC, which results from a rougher PA selective layer contributing to a thick PA selective layer.

Moreover, the AFM results shown in Fig. 12 and the results imply the surfaces of as-prepared TFC membranes are less rough compared with the substrates, which may be the result of the IP reaction and are consistent with the FESEM images. The surface roughness increases ranging from M0

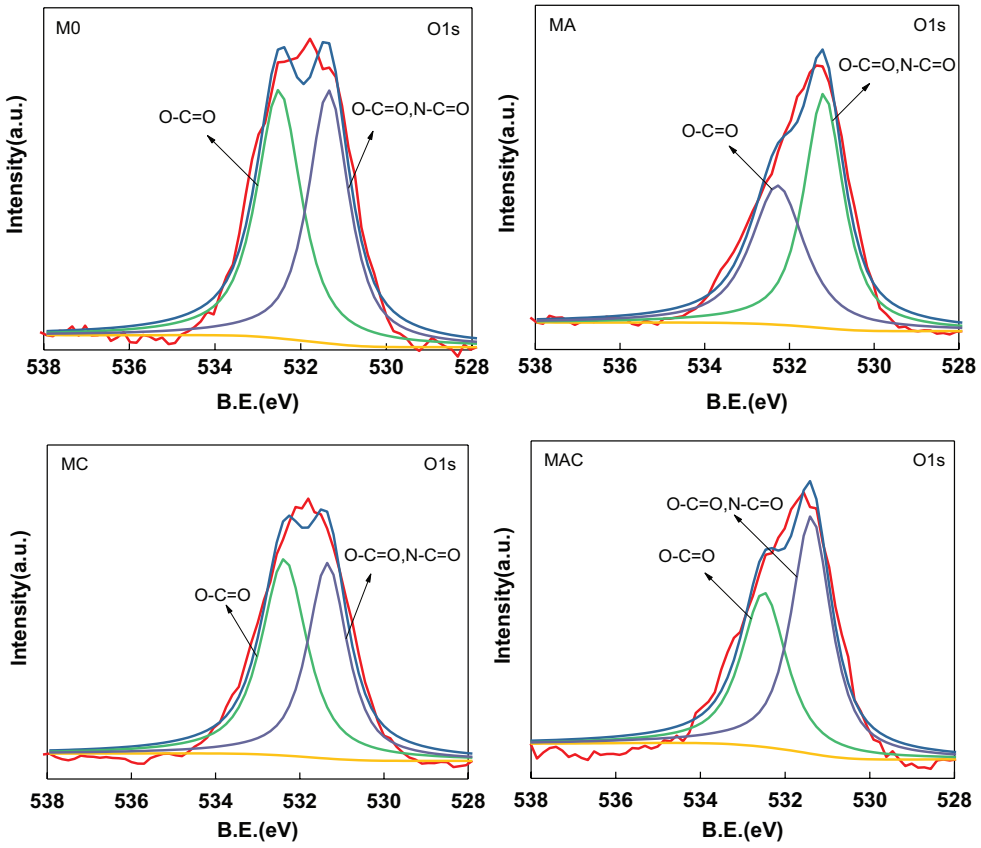

Fig. 9. High-resolution of O1s spectra of TFC membranes by XPS analysis.

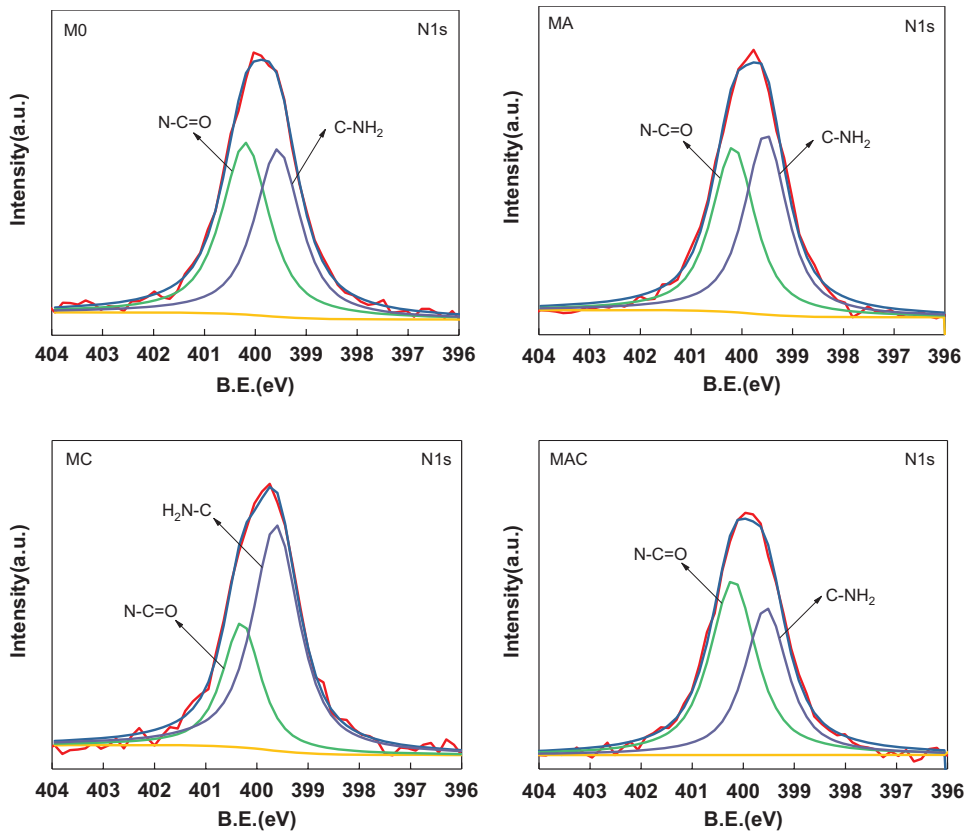

Fig. 10. High-resolution of N1s spectra of TFC membranes by XPS analysis.

Table 5
Surface chemical compositions of TFC membranes by XPS O1S spectra analysis

Membrane no.	OI	OII	OI/OII
FO-M0	4,612.882	3,422.753	1.350
FO-MA	4,711.444	3,381.689	1.390
FO-MC	4,233.876	4,290.135	0.990
FO-MAC	3,898.545	4,165.049	0.940

OI: O–C=O, N–C=O, BE = 531.2 eV.
OII: O–C=O, BE = 532.6 eV.

to MAC, which causes the higher surface roughness of the as-prepared substrates [51,52].

3.3. Influences of addition of different nanofillers on performance of TFC membranes

3.3.1. The intrinsic separation properties of the TFC membranes

As shown in Table 6, it's obvious that the water permeability parameter of the TFC membrane raises homogeneously ranging from 1.96 ± 0.27 $L \cdot m^{-2} \cdot h^{-1} \cdot bar^{-1}$ of M0 to 3.72 ± 0.16 $L \cdot m^{-2} \cdot h^{-1} \cdot bar^{-1}$ of MAC. The reason for the increase of water permeability is the improved performance of the substrates with the addition of nanofillers. In this study, we prepared highly hydrophilic, porous and badly

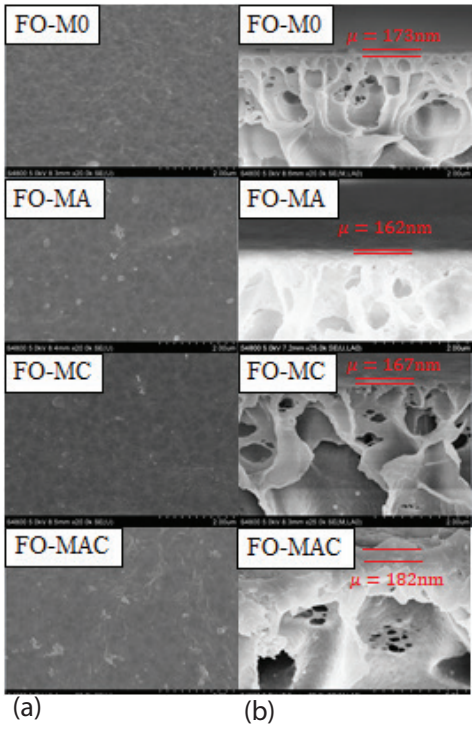

Fig. 11. FESEM images of the top surfaces (a) and cross sections (b) of the as-prepared TFC membranes.

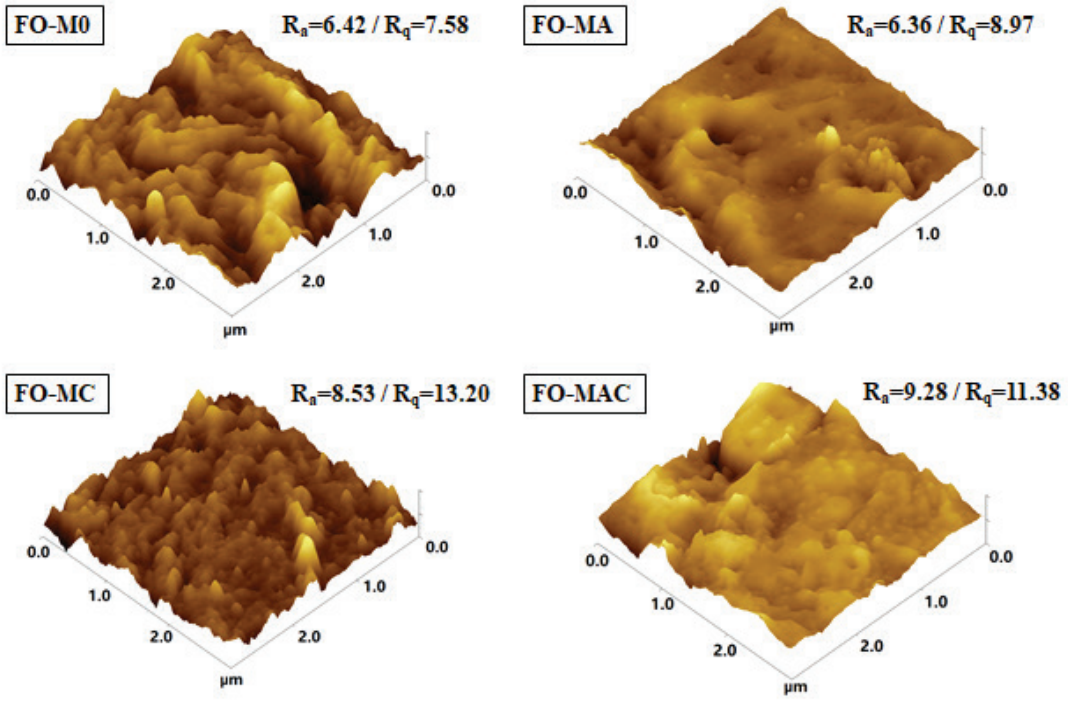

Fig. 12. AFM images of the top surfaces of the TFC membranes.

Table 6
Intrinsic separation properties of TFC membranes

Membrane no.	Rejection of NaCl (%)	A ($L \cdot m^{-2} \cdot h^{-1} \cdot bar^{-1}$)	B ($L \cdot m^{-2} \cdot h^{-1}$)	B/A (bar)
FO-M0	32.20 ± 7.14	1.96 ± 0.27	8.26 ± 0.15	4.21 ± 0.08
FO-MA	90.00 ± 1.24	2.79 ± 0.10	0.62 ± 0.07	0.23 ± 0.01
FO-MC	93.10 ± 1.94	3.31 ± 0.22	1.09 ± 0.07	0.33 ± 0.02
FO-MAC	97.60 ± 2.71	3.72 ± 0.16	0.59 ± 0.01	0.16 ± 0.00

tortuous PVDF substrate. The improved water permeability and better salt selectivity are achieved due to the great formation of the PA layer (as shown in left of Fig. 11). Table 6 demonstrates that the worst salt rejection is 32.20% ± 7.14% of M0 because the unmodified PVDF membrane has worse hydrophilicity than the modified ones, which isn't good for formation of free-defect PA layer. And the other three membranes with addition of additives into the dope solution all have higher salt rejections than the control membrane M0. The improved hydrophilicity of modified substrate is good for the formation of free-defect PA layer to enhance the salt rejection. Meanwhile, the modified TFC membranes (MA, MC, MAC) indicate lower salt permeability (B) (0.62 $L \cdot m^{-2} \cdot h^{-1}$, 1.09 $L \cdot m^{-2} \cdot h^{-1}$, 0.59 $L \cdot m^{-2} \cdot h^{-1}$) compared with the un-modified one (8.26 $L \cdot m^{-2} \cdot h^{-1}$), which also benefits from the better formation of the PA selective layer. The B/A ratio is another factor reflecting salt rejection, which reveals decrease as the increased water permeability. It is consistent with the better selectivity of the as-prepared TFC membranes.

3.3.2. Water permeability of the TFC membranes

The TFC membranes of FO-M0, FO-MA, FO-MC, FO-MAC were prepared based on the substrates of M0, MA, MC, MAC, respectively. The FO performances of the as-prepared TFC membranes in FO mode and PRO mode are measured. As is shown in Fig. 13(a), the water flux both increases in FO mode and in PRO mode from M0 to MAC, and MAC obtains the maximum water fluxes of 20.37 L and 28.23 $L \cdot m^{-2} \cdot h^{-1}$ under AL-FS and AL-DS, respectively. The improvement of the water flux may be the result of the increased hydrophilicity of the modified substrate surfaces which cuts down the permeate resistance. And a great deal of available areas for the water transport is provided by the as-prepared TFC membrane with higher surface roughness. For another thing, with the enhancive hydrophilicity of the substrates, the reverse salt flux comes down in both of AL-DS and AL-FS operation modes, which is owing to forming flawless PA selective layer as Fig. 11 shows and the result is shown in Fig. 13(b). In short,

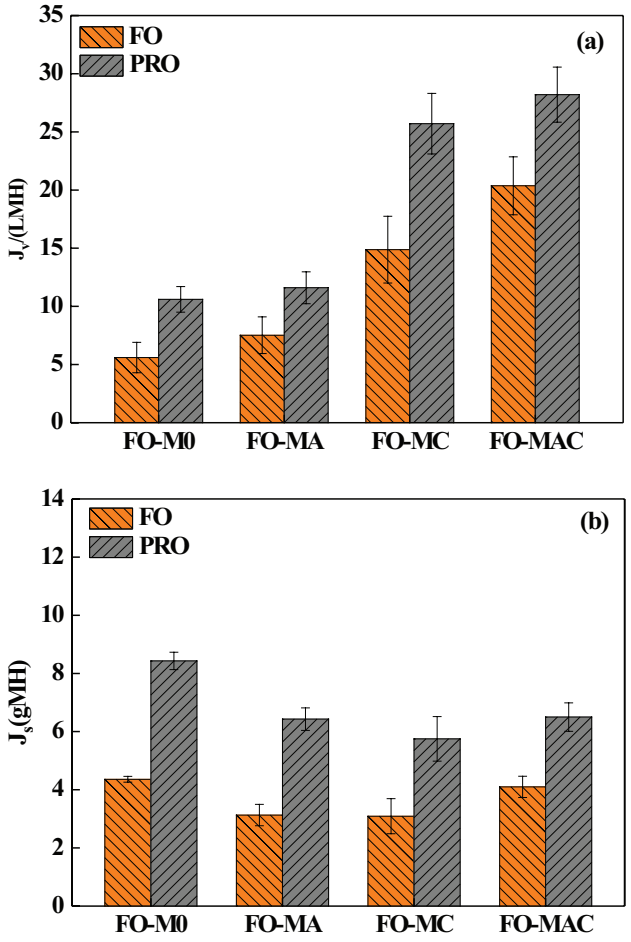

Fig. 13. FO performance of TFC membranes: (a) J_v (FO mode and PRO mode) and (b) J_s (FO mode and PRO mode) using 2 M NaCl solution as draw solution and DI water as feed solution.

the modified TFC membrane has better performance than the control membrane in this study, which further proves that blending of the hydrophilic nanofillers into the dope solution can greatly improve the performance of resultant membrane and provides a brand-new way for exploitations of substrates in FO application.

As shown in Fig. 14, it provides a new idea to evaluate the performance of TFC membrane. The water flux divided by salt flux $J_s/J_{v,}$ is used as a parameter which reflects improved selective performance of the TFC membrane during FO process and is more representative than the absolute salt flux ignoring the effect of water flux [53]. To reduce salt passing, avoid solute accumulation in feed solution and abate the supplement of the draw solution, it is of importance to keep a low solute leakage during FO process. We can see from Fig. 13 that the ratio of reverse salt flux to water flux follows the same rule as the trend of water flux and differs from the trend of reverse salt flux. The membrane MAC owns relatively low specific solute flux (0.20 and 0.23 for FO mode and PRO mode, respectively) due to its improved hydrophilicity, porous structure and better selectivity compared with other membranes.

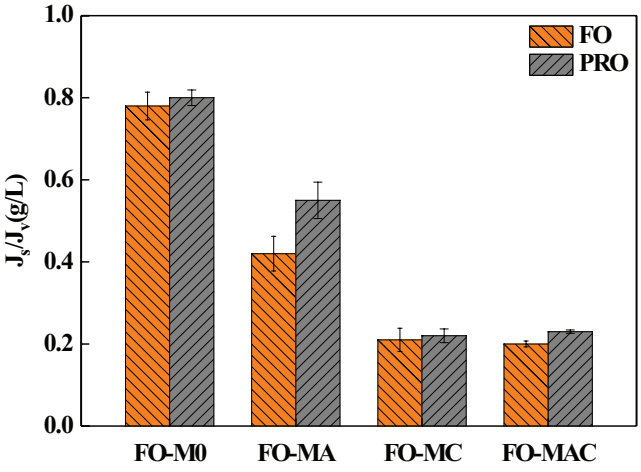

Fig. 14. Ratio of reverse solute flux and water flux of modified TFC membranes.

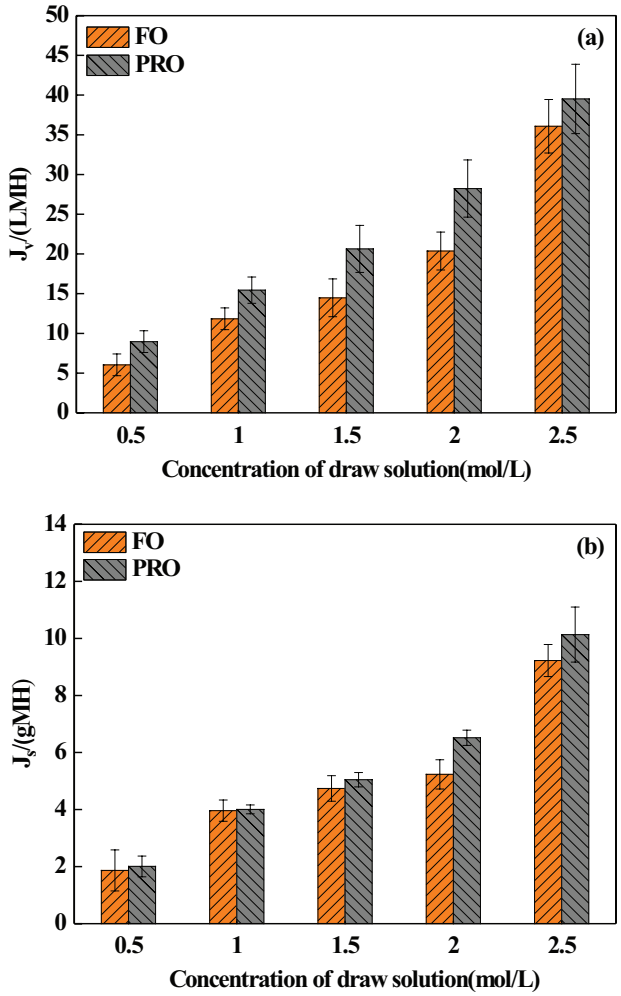

Fig. 15. FO performance of TFC membranes: (a) J_v (FO mode and PRO mode) and (b)J_s (FO mode and PRO mode) based on substrate MAC using different concentrations of NaCl solutions as draw solution, DI water as feed solution.

3.3.3. Influence of the concentration of draw solution

Fig. 15 shows the influence of concentration of draw solution osmotic pressure on the performance of TFC membranes and is discussed under two modes (FO mode and PRO mode) by using NaCl solutions ranging from 0.5 to 2.5 M as draw solution. The DI water works as feed solution. As shown in Fig. 15(a), the permeation flux is obviously enhanced with the increased osmosis pressure due to the increasing concentration of the draw solution. At the same time, the increased gradient of NaCl concentration results in the increase of the reverse salt flux [42]. Fig. 15(b) shows the same trend in PRO mode as in FO mode.

4. Conclusions

The TFC membranes based on the composite additions of AT and O-MWCNTs incorporated PVDF substrates are successfully prepared for FO application. The single and blending additions of the two materials on the intrinsic performances (pore size, porosity, thickness and hydrophilicity) of substrates and the performance (water flux, reverse slat flux and salt rejection) of corresponding TFC membranes are systematically studied. In conclusion, composite membrane with the additions of two hydrophilic nanofillers has better performance, such as improved wettability and optimized membrane morphology. Furthermore, the improvement of the salt rejection is based on the defect-free PA player formed on the hydrophilic substrate. Porous and hydrophilic substrate contributes to the higher water permeability performance of the resultant TFC membranes. The modified TFC membranes receive a higher water flux of 28.23 and 20.37 LMH in the PRO mode and FO mode, respectively and the lower reverse salt flux compared with the neat PVDF membrane.

Acknowledgements

The research is supported by Science and Technology Commission of Shanghai Municipality (13ZR1429900, 14520502900) and International Joint Laboratory of Resource Chemistry (IJLRC).

Symbols

A – Pure water permeability coefficient of TFC membrane, $L \cdot m^{-2} \cdot h^{-1} \cdot bar^{-1}$
A_m – The effective membrane area, m^2
B – Salt permeability coefficient, $L \cdot m^{-2} \cdot h^{-1}$
C_0 – The initial salt concentration, mol L^{-1}
C_d^0 – The final concentration of feed solution during FO process, mol L^{-1}
C_d^t – The final concentration of feed solution during FO process, mol L^{-1}
C_f^0 – The initial concentration of feed solution during FO process, mol L^{-1}
C_f^t – The final concentration of feed solution during FO process, mol L^{-1}
C_f – The salt concentration of the feed, mol L^{-1}
C_p – The salt concentration of permeate, mol L^{-1}
C_t – The final salt concentration, mol L^{-1}
D – The solute diffusion coefficient D, $D = 1.61 \times 10^{-9}\ m^2\ s^{-1}$
J_s – Salt flux of TFC membrane, gMH
J_v – Water flux of TFC membrane, LMH
J_w – The pure water permeation flux of the substrate, $L \cdot m^{-2} h^{-1} \cdot bar^{-1}$
l – The thickness of the substrate
ΔP – The transmembrane pressure, bar
R – Rejection for NaCl solute, %
R_a – Mean roughness of the membrane surface, nm
r_m – Average pore radius, m
R_q – Root mean square roughness, nm
t – The operation time, h
V – The volume of permeate water
V_0 – The initial volume during FO process, L
V_d – The volume of draw solution during FO process, L
V_f – The volume of the feed solution, L
V_t – The final volume during FO process, L
ΔV – The water volume from the feed solution to the draw solution over the determined operation time, L
ε – The porosity of the membranes, %
η – The water viscosity, Pa·s
μ – The thickness of active layer of the TFC membrane, μm
π_d – Osmotic pressure of the draw solution
π_f – Osmotic pressure of the feed solution
ρ_p – The density of PVDF, g/cm^3
ρ_{water} – The density of water, g/cm^3
ω_1 – The weight of the wet membrane, g
ω_2 – The weight of the dried membrane, g

References

[1] J. Zheng, M. Li, K. Yu, J. Hu, X. Zhang, L. Wang, Sulfonated multiwall carbon nanotubes assisted thin-film nanocomposite membrane with enhanced water flux and anti-fouling property, J. Membr. Sci., 524 (2017) 344–353.
[2] M. Elimelech, W.A. Phillip, The future of seawater desalination: energy, technology, and the environment, Science, 333 (2011) 712.
[3] X. Zhang, L. Shen, W.-Z. Lang, Y. Wang, Improved performance of thin-film composite membrane with PVDF/PFSA substrate for forward osmosis process, J. Membr. Sci., 535 (2017) 188–199.
[4] X. Wang, X. Wang, P. Xiao, J. Li, E. Tian, Y. Zhao, Y. Ren, High water permeable free-standing cellulose triacetate/graphene oxide membrane with enhanced antibiofouling and mechanical properties for forward osmosis, Colloids. Surf., A., 508 (2016) 327–335.
[5] R. Kaveh, Z. Shariatinia, A. Arefazar, Improvement of polyacrylonitrile ultrafiltration membranes' properties using decane-functionalized reduced graphene oxide nanoparticles, Water. Sci. Tech. Water. Supply., 16 (2016) 1378–1387.
[6] K. Goh, H.E. Karahan, L. Wei, T.-H. Bae, A.G. Fane, R. Wang, Y. Chen, Carbon nanomaterials for advancing separation membranes: a strategic perspective, Carbon, 109 (2016) 694–710.
[7] G. Chen, Z. Wang, L.D. Nghiem, X.-M. Li, M. Xie, B. Zhao, M. Zhang, J. Song, T. He, Treatment of shale gas drilling flowback fluids (SGDFs) by forward osmosis: membrane fouling and mitigation, Desalination, 366 (2015) 113–120.
[8] T.-S. Chung, S. Zhang, K.Y. Wang, J. Su, M.M. Ling, Forward osmosis processes: yesterday, today and tomorrow, Desalination, 287 (2012) 78–81.
[9] Q. Liu, J. Li, Z. Zhou, J. Xie, J.Y. Lee, Hydrophilic Mineral coating of membrane substrate for reducing internal concentration polarization (ICP) in forward osmosis, Sci. Rep., 6 (2016) 19593.
[10] X. Li, C.H. Loh, R. Wang, W. Widjajanti, J. Torres, Fabrication of a robust high-performance FO membrane by optimizing substrate structure and incorporating aquaporin into selective layer, J. Membr. Sci., 525 (2017) 257–268.

[11] D. Li, Y. Yan, H. Wang, Recent advances in polymer and polymer composite membranes for reverse and forward osmosis processes, Prog. Polym. Sci., 61 (2016) 104–155.
[12] J.n. Shen, C.c. Yu, H.m. Ruan, C.j. Gao, B. Van der Bruggen, Preparation and characterization of thin-film nanocomposite membranes embedded with poly(methyl methacrylate) hydrophobic modified multiwalled carbon nanotubes by interfacial polymerization, J. Membr. Sci., 442 (2013) 18–26.
[13] K.Y. Wang, T.-S. Chung, G. Amy, Developing thin-film-composite forward osmosis membranes on the PES/SPSf substrate through interfacial polymerization, AIChE. J., 58 (2012) 770–781.
[14] H. Hoseinpour, M. Jahanshahi, M. Peyravi, A. Nozad, Feasibility study of a novel copolyamide thin film composite membrane assisted by melamine in terms of acid and thermal stability, J. Ind. Eng. Chem., 46 (2017) 244–257.
[15] M. Tian, Y.-N. Wang, R. Wang, Synthesis and characterization of novel high-performance thin film nanocomposite (TFN) FO membranes with nanofibrous substrate reinforced by functionalized carbon nanotubes, Desalination, 370 (2015) 79–86.
[16] Y. Wang, R. Ou, Q. Ge, H. Wang, T. Xu, Preparation of polyethersulfone/carbon nanotube substrate for high-performance forward osmosis membrane, Desalination, 330 (2013) 70–78.
[17] M. Tian, Y.-N. Wang, R. Wang, A.G. Fane, Synthesis and characterization of thin film nanocomposite forward osmosis membranes supported by silica nanoparticle incorporated nanofibrous substrate, Desalination, 401 (2017) 142–150.
[18] M.J. Park, S. Phuntsho, T. He, G.M. Nisola, L.D. Tijing, X.-M. Li, G. Chen, W.-J. Chung, H.K. Shon, Graphene oxide incorporated polysulfone substrate for the fabrication of flat-sheet thin-film composite forward osmosis membranes, J. Membr. Sci., 493 (2015) 496–507.
[19] P. Xiao, L.D. Nghiem, Y. Yin, X.-M. Li, M. Zhang, G. Chen, J. Song, T. He, A sacrificial-layer approach to fabricate polysulfone support for forward osmosis thin-film composite membranes with reduced internal concentration polarisation, J. Membr. Sci., 481 (2015) 106–114.
[20] H. Jin, Y. Huang, X. Wang, P. Yu, Y. Luo, Preparation of modified cellulose acetate membranes using functionalized multi-walled carbon nanotubes for forward osmosis, Desal. Wat. Treat., 57 (2015) 7166–7174.
[21] G. Li, X.-M. Li, T. He, B. Jiang, C. Gao, Cellulose triacetate forward osmosis membranes: preparation and characterization, Desal. Wat. Treat., 51 (2013) 2656–2665.
[22] M. Amini, M. Jahanshahi, A. Rahimpour, Synthesis of novel thin film nanocomposite (TFN) forward osmosis membranes using functionalized multi-walled carbon nanotubes, J. Membr. Sci., 435 (2013) 233–241.
[23] D. Emadzadeh, W.J. Lau, A.F. Ismail, Synthesis of thin film nanocomposite forward osmosis membrane with enhancement in water flux without sacrificing salt rejection, Desalination, 330 (2013) 90–99.
[24] G. Chen, Z. Wang, X.-M. Li, J. Song, B. Zhao, S. Phuntsho, H.K. Shon, T. He, Concentrating underground brine by FO process: influence of membrane types and spacer on membrane scaling, Chem. Eng. J., 285 (2016) 92–100.
[25] A.F. Ismail, N.H. Rahim, A. Mustafa, T. Matsuura, B.C. Ng, S. Abdullah, S.A. Hashemifard, Gas separation performance of polyethersulfone/multi-walled carbon nanotubes mixed matrix membranes, Sep. Purif. Technol., 80 (2011) 20–31.
[26] G. Chen, X.-M. Li, M. Huang, T. He, Concentrating underground brine using a TFC hollow fiber forward osmosis membrane: effects of cleaning, Environ. Sci., 4 (2018) 851–862.
[27] M. Cho, S.H. Lee, D. Lee, D.P. Chen, I.-C. Kim, M.S. Diallo, Osmotically driven membrane processes: exploring the potential of branched polyethyleneimine as draw solute using porous FO membranes with NF separation layers, J. Membr. Sci., 511 (2016) 278–288.
[28] K. Lutchmiah, A.R. Verliefde, K. Roest, L.C. Rietveld, E.R. Cornelissen, Forward osmosis for application in wastewater treatment: a review, Water. Res., 58 (2014) 179–197.
[29] V. Vatanpour, M. Esmaeili, M.H.D.A. Farahani, Fouling reduction and retention increment of polyethersulfone nanofiltration membranes embedded by amine-functionalized multi-walled carbon nanotubes, J. Membr. Sci., 466 (2014) 70–81.
[30] Y. Wang, R. Ou, H. Wang, T. Xu, Graphene oxide modified graphitic carbon nitride as a modifier for thin film composite forward osmosis membrane, J. Membr. Sci., 475 (2015) 281–289.
[31] L. Xiang, Y. Pan, G. Zeng, J. Jiang, J. Chen, C. Wang, Preparation of poly(ether-block-amide)/attapulgite mixed matrix membranes for CO_2/N_2 separation, J. Membr. Sci., 500 (2016) 66–75.
[32] W. Wang, J. Fang, S. Shao, M. Lai, C. Lu, Compact and uniform TiO_2 @g-C_3 N_4 core-shell quantum heterojunction for photocatalytic degradation of tetracycline antibiotics, Appl. Catal. B., 217 (2017) 57–64.
[33] C. Zhang, K. Wei, W. Zhang, Y. Bai, Y. Sun, J. Gu, Graphene oxide quantum dots incorporated into a thin film nanocomposite membrane with high flux and antifouling properties for low-pressure nanofiltration, ACS. Appl. Mater. Interface., 9 (2017) 11082–11094.
[34] H. Kang, W. Wang, J. Shi, Z.W. Xu, H.M. Lv, X.M. Qian, L.Y. Liu, M.L. Jing, F.Y. Li, J.R. Niu, Interlamination restrictive effect of carbon nanotubes for graphene oxide forward osmosis membrane via layer by layer assembly, Appl. Surf. Sci., 465 (2019) 1103–1106.
[35] C. Liu, X. Lei, L. Wang, J. Jia, X. Liang, X. Zhao, H. Zhu, Investigation on the removal performances of heavy metal ions with the layer-by-layer assembled forward osmosis membranes, Chem. Eng. J., 327 (2017) 60–70.
[36] L. Setiawan, R. Wang, K. Li, A.G. Fane, Fabrication of novel poly(amide–imide) forward osmosis hollow fiber membranes with a positively charged nanofiltration-like selective layer, J. Membr. Sci., 369 (2011) 196–205.
[37] A. Shakeri, H. Salehi, M. Rastgar, Chitosan-based thin active layer membrane for forward osmosis desalination, Carbohydr. Polym., 174 (2017) 658–668.
[38] Z.C. Yang, M. Wang, A.M. Yong, S.Y. Wong, X.H. Zhang, H. Tan, A.Y. Chang, X. Li, J. Wang, Intrinsically fluorescent carbon dots with tunable emission derived from hydrothermal treatment of glucose in the presence of monopotassium phosphate, Chem. Comm (Camb)., 47 (2011) 11615–11617.
[39] C.D. Hatch, J.S. Wiese, C.C. Crane, K.J. Harris, H.G. Kloss, J. Baltrusaitis, Water adsorption on clay minerals as a function of relative humidity: application of BET and Freundlich adsorption models, Langmuir, 28 (2012) 179–803.
[40] M. Safarpour, A. Khataee, V. Vatanpour, Preparation of a novel polyvinylidene fluoride (PVDF) ultrafiltration membrane modified with reduced graphene oxide/titanium dioxide (TiO_2) nanocomposite with enhanced hydrophilicity and antifouling properties, Ind. Eng. Chem. Res., 53 (2014) 13370–13382.
[41] H. Dong, L. Zhao, L. Zhang, H. Chen, C. Gao, W.S. Winston Ho, High-flux reverse osmosis membranes incorporated with NaY zeolite nanoparticles for brackish water desalination, J. Membr. Sci., 476 (2015) 373–383.
[42] J. Ji, S. Zhou, C.Y. Lai, B. Wang, K. Li, PVDF/palygorskite composite ultrafiltration membranes with enhanced abrasion resistance and flux, J. Membr. Sci., 495 (2015) 91–100.
[43] M. Norouzi, M. Pakizeh, M. Namvar-Mahboub, The Effect of highly dispersed oxidized multi-walled carbon nanotubes on the performance of PVDF/PVC ultrafiltration membrane, Desal. Wat. Treat., 57 (2016) 24778–24787.
[44] P.H. Duong, S. Chisca, P.Y. Hong, H. Cheng, S.P. Nunes, T.S. Chung, Hydroxyl functionalized polytriazole-co-polyoxadiazole as substrates for forward osmosis membranes, ACS. Appl. Mater. Interfaces., 7 (2015) 3960–3973.
[45] M. Fathizadeh, A. Aroujalian, A. Raisi, Effect of lag time in interfacial polymerization on polyamide composite membrane with different hydrophilic sub layers, Desalination, 284 (2012) 32–41.
[46] P. Cruz-Tato, E.O. Ortiz-Quiles, K. Vega-Figueroa, L. Santiago-Martoral, M. Flynn, L.M. Diaz-Vazquez, E. Nicolau, Metalized nanocellulose composites as a feasible material for membrane

supports: design and applications for water treatment, Environ. Sci. Technol., 51 (2017) 4585–4595.
[47] J.L. Xinzhen Zhao, Changkun Liu, A novel TFC-type FO membrane with inserted sublayer of carbon nanotube networks exhibiting the improved separation performance, Desalination, 413 (2017) 176–183.
[48] M. Tian, C. Qiu, Y. Liao, S. Chou, R. Wang, Preparation of polyamide thin film composite forward osmosis membranes using electrospun polyvinylidene fluoride (PVDF) nanofibers as substrates, Sep. Purif. Technol., 118 (2013) 727–736.
[49] L. Shen, J. Zuo, Y. Wang, Tris(2-aminoethyl)amine in-situ modified thin-film composite membranes for forward osmosis applications, J. Membr. Sci., 537 (2017) 186–201.
[50] C. Klaysom, S. Hermans, A. Gahlaut, S. Van Craenenbroeck, I.F.J. Vankelecom, Polyamide/polyacrylonitrile (PA/PAN) thin film composite osmosis membranes: film optimization, characterization and performance evaluation, J. Membr. Sci., 445 (2013) 25–33.
[51] D.R.a.T. Matsuura, Surface Modifications for Antifouling Membranes, Chem. Rev., 110 (2010) 24.
[52] M. Ghanbari, D. Emadzadeh, W.J. Lau, H. Riazi, D. Almasi, A.F. Ismail, Minimizing structural parameter of thin film composite forward osmosis membranes using polysulfone/halloysite nanotubes as membrane substrates, Desalination, 377 (2016) 152–162.
[53] W. Fang, R. Wang, S. Chou, L. Setiawan, A.G. Fane, Composite forward osmosis hollow fiber membranes: integration of RO- and NF-like selective layers to enhance membrane properties of anti-scaling and anti-internal concentration polarization, J. Membr. Sci., 394–395 (2012) 140–150.